



19 **Abstract**

20 Constraining the long-term variability and average of the Earth’s magnetic field  
 21 strength is fundamental to understanding the characteristics and behavior of the geo-  
 22 magnetic field. Questions remain about the strength of the average field, and the rela-  
 23 tionship between strength and reversal frequency. The dispersion of data from key time  
 24 intervals reflects the complexity in obtaining absolute paleointensity values. Here, we fo-  
 25 cus on the Cretaceous Normal Superchron (CNS; 121-84 Ma), during which there were  
 26 no reversals. We present new results from 42 submarine basaltic glass (SBG) sites col-  
 27 lected on the Nicoya Peninsula and Murciélago Islands, Costa Rica and new and revised  
 28  $^{40}\text{Ar}/^{39}\text{Ar}$  ages along with biostratigraphic age constraints from previous studies that  
 29 indicate ages ranging from 141 to 112 Ma. One site with a  $^{40}\text{Ar}/^{39}\text{Ar}$  age of  $135 \pm 1.5$   
 30 Ma ( $2\sigma$ ) gave a reliable intensity result of  $34 \pm 8 \mu\text{T}$  (equivalent to a paleomagnetic dipole  
 31 moment, PDM, value of  $88 \pm 20 \text{ZAm}^2$ ), while three sites between 121 and 112 vary from  
 32  $21 \pm 1$  to  $34 \pm 4 \mu\text{T}$  ( $53 \pm 3$  to  $87 \pm 10 \text{ZAm}^2$ ) spanning the onset of the CNS. These  
 33 results from the CNS are all higher than the long-term average of  $\sim 42 \text{ZAm}^2$  and simi-  
 34 lar to data from Suhongtu ( $46\text{-}53 \text{ZAm}^2$ ) and the Troodos Ophiolite ( $81 \text{ZAm}^2$ , rein-  
 35 terpreted using the same criteria of this study). Together with the reinterpreted data,  
 36 the new Costa Rica results suggest that the strength of the geomagnetic field was about  
 37 the same before and after the onset of the CNS. Therefore, the data do not support a  
 38 strict correlation between polarity interval length and the strength of the magnetic field.

39 **Plain language summary**

40 Understanding the Earth’s magnetic field behavior in the past is important for geo-  
 41 dynamo simulations. However, because of the paucity of available data, it is poorly un-  
 42 derstood. In particular, it has been argued that the strength of the Earth’s magnetic field,  
 43 or paleointensity, seems correlated with the stability of the field, where a strong field may  
 44 be less prone to magnetic reversals than a weak field. Hence, we have investigated the  
 45 anomalously long period of stability, the Cretaceous Normal Superchron (CNS) during  
 46 which no magnetic reversals occurred. Our new data from Costa Rica basaltic glasses,  
 47 together with reinterpreted data from the Suhongtu lavas in Mongolia, Troodos ophi-  
 48 olite in Cyprus suggest that the magnetic field during the CNS was similar to the present  
 49 day field and these high values are nearly twice the long-term average value. However,  
 50 high field values were also detected in the period prior to the onset of the CNS as well,  
 51 hence our data do not support a strict correlation between strength and stability of the  
 52 Earth’s magnetic field.

53 **1 Introduction**

54 From the analysis of satellite data, we observe a rapid decrease of the present-day  
 55 Earth’s magnetic (geomagnetic) field strength (intensity), thus raising the question of  
 56 whether we are approaching a polarity reversal (e.g. Hulot et al., 2002; Pavón-Carrasco  
 57 & De Santis, 2016) or not (Brown et al., 2018). Constraining the past evolution of in-  
 58 tensity (paleointensity) can provide context for this scenario, and help us to understand  
 59 fundamental properties of the geomagnetic field, such as the long-term average dipole  
 60 moment and how the field’s strength is related to reversals, reversal frequency and sec-  
 61 ular variation (e.g. Cox, 1968).

62 Generally, paleointensity minima are associated with magnetic excursions and re-  
 63 versals but they are not always associated with these events (Channell et al., 2020). Iden-  
 64 tifying a relationship between dipole strength and magnetic reversals (Biggin & Thomas,  
 65 2003; Biggin et al., 2012; Constable et al., 1998; Cox, 1968; Ingham et al., 2014; Kulakov  
 66 et al., 2019; Larson & Olson, 1991; Loper & McCartney, 1986; McElhinny & Larson, 2003;  
 67 Prévot et al., 1990; Selkin & Tauxe, 2000; Tarduno et al., 2001; Tarduno & Cottrell, 2005;

68 Tauxe, 2006; Tauxe et al., 2013; Tauxe & Yamazaki, 2015; Thomas et al., 1998, 2000)  
 69 would provide important constraints on the heat flux across the Earth’s core-mantle bound-  
 70 ary and the energy states of the geodynamo. These in turn would have significant im-  
 71 plications for the geodynamo and mantle modeling (Biggin et al., 2012). Moreover, un-  
 72 derstanding the long-term variations of the geomagnetic field strength (McFadden & McEl-  
 73 hinny, 1982; Juarez et al., 1998; Wang et al., 2015; Tauxe et al., 2013; Kulakov et al.,  
 74 2019; Ingham et al., 2014) over thousands to millions of years is not only fundamental  
 75 for modelling the geodynamo origin and behavior (e.g. Biggin et al., 2012) but also for  
 76 other applications, such as estimating the solar standoff distance (Tarduno et al., 2014)  
 77 or geodynamic plate reconstructions (e.g. Olierook et al., 2020). However, there is no  
 78 consensus yet as to the average strength of the geomagnetic field, with estimates rang-  
 79 ing from  $80 \pm 7 \text{ ZAm}^2$  (where  $\text{ZAm}^2 = 10^{21} \text{ Am}^2$ ) for the last 5 Ma (McFadden & McEl-  
 80 hinny, 1982), to  $42 \pm 23 \text{ ZAm}^2$  for the last 160 Ma (all intensity values errors are  $1\sigma$ ;  
 81 Juarez et al., 1998).

82 Despite the many compilations associated with the strength of the geomagnetic field  
 83 over time (e.g. Biggin & McCormack, 2010; Perrin & Schnepp, 2004; Perrin & Shcherbakov,  
 84 1997; Tanaka et al., 1995; Tauxe & Yamazaki, 2015, and earthref.org/MagIC), the data  
 85 distribution is uneven both geographically and temporally. Overall,  $\sim 95\%$  of the data  
 86 in the MagIC database (combining both volcanic and archeomagnetic records) comes from  
 87 northern hemisphere locations, whereas only  $\sim 5\%$  comes from southern latitudes. More-  
 88 over, most of the data comes from the last 20,000 years. This significant bias in geographic  
 89 and temporal span is due to: i) the limited availability of suitable materials for paleo-  
 90 magnetic analyses, as older rocks with ideal characteristics are much less common than  
 91 younger rocks, and ii) the high-failure rate and time-consuming nature of the paleoin-  
 92 tensity experiments. The scatter in the database may be also increased by low resolu-  
 93 tion of geochronological dating methods (the uncertainties can range from hundreds to  
 94 millions of years).

95 A way to advance our understating of geomagnetic field activity and mantle dy-  
 96 namics is to investigate the superchrons, intervals of tens of millions of years that lack  
 97 reversals. Gubbins (1999) proposed that excursions and reversals nucleate in the fluid  
 98 outer core and if the reverse outer core field is maintained for longer than about 3 ka (the  
 99 magnetic diffusion time of the inner core) then the field is able to diffuse into the inner  
 100 core, allowing the dipole field to reverse. This hypothesis may explain the existence and  
 101 relatively short duration of the magnetic excursions, which are thousands of years long.  
 102 In contrast, superchrons may be related to the relationship between the Earth’s dynamo  
 103 and the lower mantle (Glazmaier et al., 1999; Larson & Olson, 1991; Olson et al., 2012)  
 104 or they can be triggered by crustal/upper mantle events, such as an impingement of a  
 105 subducted slab with the core–mantle boundary (Courtilot et al., 2007; Larson & Olson,  
 106 1991).

107 If the long-term thermal effect of mantle convection on the core during the Cre-  
 108 taceous led to a gradual decrease of the reversal rate before the onset of the superchron,  
 109 then its existence could be predicted (McFadden & McElhinny, 1984; McFadden & Mer-  
 110 rill, 2000). Alternatively, if the reversal rate was stationary before the superchron (Gallet  
 111 & Hulot, 1997; Hulot & Gallet, 2003), then it could represent a sudden non-linear tran-  
 112 sition between a reversing and a non-reversing state of the geodynamo and the CNS could  
 113 not be predicted (de-coupling between core-mantle processes and geomagnetic field long  
 114 term changes, Prévot et al., 1990). Furthermore, numerical simulations by Olson and Ha-  
 115 gay (2015) suggested that superchrons are induced by mantle ‘superplume’ activity. These  
 116 are manifested by major Large Igneous Provinces (LIPs), the age of which post-date tran-  
 117 sitions from hyper-reversing (i.e. the Jurassic Hyperactivity Period, JHP, Kulakov et al.,  
 118 2019) to superchron geodynamo states (i.e., the CNS). Therefore, improving our knowl-  
 119 edge of the timing and extent of LIPs could help constraining the geomagnetic field be-  
 120 havior. Finding a precursor event to a superchron would support one of the competing

121 hypotheses over the others (Gallet & Hulot, 1997; Hulot & Gallet, 2003; Zhu, Hoffman,  
 122 et al., 2004). The key to this is to expand the existing sparse database spanning the on-  
 123 set of a superchron (here the CNS). In this study, we focus on obtaining new and robust  
 124 data from before and after the onset of the CNS, from the study of part of the Caribbean  
 125 Large Igneous Province (CLIP: e.g., Boshman et al., 2019) in Costa Rica.

## 126 2 The Cretaceous Normal Superchron (CNS)

127 The Cretaceous Normal Superchron (C34n; informally called ‘the Cretaceous quiet  
 128 zone’, e.g., Gee & Kent, 2007) is a long period of nearly uniform normal polarity, first  
 129 observed by Helsley and Steiner (1968) in ocean-floor magnetic anomaly profiles. The  
 130 CNS began between 123.0 and 121.2 Ma, with a duration of 38.0 to 40.5 Ma (see review  
 131 by Olierook et al., 2020), and it provides a unique opportunity to investigate the geo-  
 132 magnetic field behavior before, during, and after a superchron. Indeed, the CNS is pre-  
 133 ceded by the so-called ‘Mesozoic dipole low’ (Prévot et al., 1990) with an average inten-  
 134 sity value of  $\sim 32 \text{ ZAm}^2$  (e.g. Tauxe et al., 2013), possibly linked to a change of state of  
 135 the geomagnetic field from a state of relatively rapid reversals, to a period of stability  
 136 during the CNS. Cox (1968) suggested that when the field is stronger, it is also more sta-  
 137 ble and therefore the frequency of reversals should be lower. Many subsequent studies  
 138 have supported the inverse correlation between field strength and reversal frequency (e.g.  
 139 Constable et al., 1998; Tauxe & Hartl, 1997; Tauxe & Staudigel, 2004; Tauxe, 2006; Tauxe  
 140 & Yamazaki, 2015; Kulakov et al., 2019), whereas others (e.g. Selkin & Tauxe, 2000) sug-  
 141 gested that the distribution of paleointensities does not change substantially between a  
 142 low reversal-rate period (e.g., between 124 and 30 Ma) and a high reversal-rate period  
 143 (e.g., between 30 and 0.3 Ma).

144 At present, too few data are available to rule out either of these hypotheses, as sug-  
 145 gested by Ingham et al. (2014). The investigation of SBG samples from the Troodos ophi-  
 146 olite in Cyprus (92 Ma, Tauxe & Staudigel, 2004) suggest that a strong and stable field  
 147 was present during the CNS, with a mean dipole moment of  $81 \pm 43 \text{ ZAm}^2$ . An even  
 148 higher dipole moment values of  $125 \pm 14 \text{ ZAm}^2$  was recovered from single plagioclase  
 149 crystals extracted from the Rajmahal Traps of India (113 to 116 Ma; Cottrell & Tarduno,  
 150 2000; Tarduno et al., 2001) and  $127 \pm 7 \text{ ZAm}^2$  from the Canadian Arctic Ellesmere Is-  
 151 land 95 Ma lavas (Tarduno et al., 2002). High values were later supported by the review  
 152 of paleointensity data from all SBG samples (up to 2006) from Deep Sea Drilling Project  
 153 and Ocean Drilling Program (DSDP/ODP) core samples (Tauxe, 2006).

154 Alternatively, there are many studies that suggest relatively low field values dur-  
 155 ing the whole period of the CNS. Data from the lower crust (gabbros) of the Troodos  
 156 ophiolite by Granot et al. (2007) pointed to fluctuations of the intensities around a mean  
 157 of  $54 \pm 20 \text{ ZAm}^2$ , which are weaker and more variable than predicted by geodynamo sim-  
 158 ulations. Low intensity values were also observed from the 114-110 Ma Suhongtu lava  
 159 section (Inner Mongolia) by Zhu et al. (2008) who found a field that fluctuated from  $53$   
 160  $\pm 20 \text{ ZAm}^2$  to  $46 \pm 27 \text{ ZAm}^2$ . Similar low intensity values were also found by Pick  
 161 and Tauxe (1993a) after analyzing SBG samples from the East Pacific Rise DSDP/ODP sites  
 162 spanning the onset of the CNS (Holes 417D, 418A, 807C), and near the CNS termina-  
 163 tion (Hole 543A). A precursor event to the CNS has been proposed by Gallet and Hu-  
 164 lot (1997) and Hulot and Gallet (2003), and supported by values of  $64 \pm 23 \text{ ZAm}^2$  at  
 165 134 Ma from Uruguay (e.g. Goguitchaichvili et al., 2008). Moreover, data from the Zhuanchengzi  
 166 in Liaoning Province, K-Ar dated at  $120.93 \pm 0.88 \text{ Ma}$  (all age uncertainties are  $2\sigma$  un-  
 167 less otherwise stated) closely following the onset of the CNS, reveal a low average inten-  
 168 sity of  $39.6 \pm 0.8 \text{ ZAm}^2$  (Zhu et al., 2001). An even weaker field was reported from the  
 169 southern hemisphere, with data from 135 Ma old lava flows from the Etendeka-Paraná  
 170 Province (Dodd et al., 2015), with an average of  $25 \pm 10 \text{ ZAm}^2$ . Similar low values of  
 171  $41 \pm 16 \text{ ZAm}^2$  (and high variability) were found on the South American part of the same  
 172 province, in the 130 Ma Ponta Grossa tholeiitic dykes (Cejudo Ruiz et al., 2009), from

173 a sequence of 124-133 Ma lava flows at Sihetun (Zhu et al., 2004a) and 122 Ma andesitic  
174 basalt lava flows from Hulahada, northeastern China (Zhu et al., 2004b). Thus, these  
175 data (Zhu et al., 2001, 2003; Zhu, Lo, et al., 2004; Cejudo Ruiz et al., 2009; Dodd et al.,  
176 2015) suggest that no precursor to the CNS was recorded and the field was weak both  
177 prior to ( $35.3 \pm 0.2 \text{ ZAm}^2$ ) and after ( $48 \pm 0.2 \text{ ZAm}^2$ ) the CNS. These low intensities  
178 would support a decoupling of the processes controlling reversal frequency and paleoin-  
179 tensity.

180 There is also a discrepancy between magnetic anomalies, volcanic and sedimentary  
181 data (Tarduno, 1990; Cronin et al., 2001; Granot et al., 2012) during the CNS. For ex-  
182 ample, Granot et al. (2012) discovered two magnetic anomalies within the CNS (with  
183 higher intensity values at  $\sim 108$  Ma, and lower at  $\sim 92$  Ma) from deep-tow magnetic pro-  
184 files from the Central Atlantic Ocean, which are not observed in the volcanic or sedimen-  
185 tary data.

186 Kulakov et al. (2019) analyzed data from the PINT (Paleo-INTensity) dataset (Biggin  
187 & McCormack, 2010), to investigate the variability of the geomagnetic field and rever-  
188 sal frequency between the CNS and the JHP; they found a weak inverse correlation us-  
189 ing the entire dataset, which is in agreement with Channell et al. (1982) and Tarduno  
190 and Cotrell (2005). However, when using a stricter selection criteria, no correlation was  
191 found. Overall, Kulakov et al. (2019) found an increase of field strength at  $\sim 133$  Ma,  
192 before the onset of the CNS, which lasted up to 15 Ma after the end of the CNS, and  
193 two peaks at  $\sim 117$  and  $\sim 95$  Ma, reminiscent of the findings of Granot et al. (2012). Kulakov  
194 et al. (2019) also pointed out that material from which the paleointensity data were re-  
195 covered may also bias the results as data from single zircons are systematically higher  
196 with less variability compared to data from SBG and whole rock samples, while SBG give  
197 more dispersed values with lower median values. However, we note that overall there are  
198 very few single crystal results and the results have never been verified by measuring sam-  
199 ples cooled in known fields, whereas SBG has been verified multiple times.

200 SBG is rapidly cooled, is likely to have single domain magnetic particles (Pick &  
201 Tauxe, 1993a, 1993b; Bowles et al., 2005), and may yield results that meet stricter cri-  
202 teria than in other materials. SBG has been the subject of many paleointensity stud-  
203 ies (e.g. Bowles et al., 2005; Juarez et al., 1998; Juarez & Tauxe, 2000; Pick & Tauxe,  
204 1993a; Riisager et al., 2003; Selkin & Tauxe, 2000; Smirnov & Tarduno, 2003; Tauxe &  
205 Staudigel, 2004; Tauxe et al., 2013) and their reliability has been thoroughly discussed.  
206 For instance, Smirnov and Tarduno (2003) compared the rock magnetic properties and  
207 behavior of a few specimens during heating (as required for running Thellier experiments)  
208 on Holocene and Cretaceous SBG and concluded that the magnetic behavior of their spec-  
209 imens was not comparable, pointing out that partial melting and neo-crystallization of  
210 magnetic grains would bias the results toward lower values. On the other hand, Tauxe  
211 and Staudigel (2004) argued that SBG are resistant under some conditions; indeed, the  
212 susceptibility of volcanic glasses to weathering may cause the alteration of the glass into  
213 hydrous phases that would in turn rapidly disappear from the geological record. Nonethe-  
214 less, fresh-looking samples are still found in abundance in outcrops (e.g. Tauxe & Staudi-  
215 gel, 2004) and drill cores (e.g. Selkin & Tauxe, 2000; Tauxe, 2006). These glasses also  
216 give paleointensity results that meet strict criteria, thus suggesting magnetic stability  
217 over millions of years. In contrast, Heller et al. (2002) argued for a low temperature ori-  
218 gin of low-Ti titanomagnetite, because it cannot be found as equilibrium phase in Mid  
219 Oceanic Ridge basalts. However, three important pieces of evidence argue otherwise: 1)  
220 low-Ti titanomagnetite is found in freshly erupted material, 2) several successful pale-  
221 ointensity experiments from historical flows clearly show blocking temperatures from 430  
222 to  $575^\circ\text{C}$  (Bowles et al., 2011; Carlut & Kent, 2000; Juarez et al., 1998; Kent & Gee, 1996;  
223 Pick & Tauxe, 1993a; Tauxe et al., 2013), which yielded values in good agreement with  
224 the known field from the eruptions, and 3) glass is by definition not an equilibrium ma-  
225 terial, so the argument of Heller et al. (2002) is irrelevant. Finally, as volcanic glasses

cool rapidly (are quenched) below the Curie temperatures (Bowles et al., 2005), little or no cooling rate correction needs to be applied to the final data when acquired by rapid cooling (as observed in the Scripps Paleomagnetic Laboratory).

Here, we present new and robust results obtained from SBG samples from Costa Rica (the Nicoya Peninsula and Murciélago Islands). These new data, combined with previous studies that provided geochronological and biostratigraphic ages between 141 and 94 Ma, give us the opportunity to investigate the geomagnetic field strength before and during the CNS.

### 3 Geological setting and sampling

Costa Rica is located near the triple junction of the Cocos, Caribbean and Nazca plates (DeMets, 2001), where the Cocos Plate subducts beneath the Caribbean Plate at a rate of  $\sim 8.5$  cm yr<sup>-1</sup>. For this study, we focus on the Nicoya Peninsula and Murciélago islands in the north west (10° N; 85° W, Figure 1), where an important ophiolitic complex exposes upper crust sequences and overlying sediments. The Nicoya Peninsula comprises Cretaceous aphyric pillow lavas and lava flows (dated by <sup>40</sup>Ar/<sup>39</sup>Ar), which are associated with the formation of the Jurassic-Cretaceous CLIP (Sinton et al., 1997; Hauff et al., 2000; Hoernle et al., 2004; Madrigal et al., 2016). The crustal basaltic sequence is locally intruded by late Cretaceous diabbases, gabbros and plagiogranites dated by <sup>40</sup>Ar/<sup>39</sup>Ar and U-Pb methods (Hauff et al., 2000; Madrigal et al., 2016; Sinton et al., 1997; Whatam & Stern, 2016) and by analyses of dismembered radiolaritic chert sequences from the Middle Jurassic to Late Cretaceous (Baumgartner, 1984; Schmidt-Effing, 1975, 1979; Bandini et al., 2008; Baumgartner et al., 1995). There are rare occurrences of fossil-bearing intra-pillow sediments indicating an age of  $\sim 94$  Ma (Azema et al., n.d.; Tournon & Alvarado, 1997).

Three extrusive lava sequences are recognised, which are chronologically divided into three main events: Nicoya I ( $\sim 140$  Ma), Nicoya II ( $\sim 120$  Ma) and Nicoya III ( $\sim 90$  Ma; Hoernle et al., 2004; Madrigal et al., 2016). These are considered to be part of the CLIP and a remnant of the Panthalassa Ocean. The lava sequences preserve fresh pillow-rim glasses (Figures 1 and 2). The lack of vesicularity in the lava flows and the high sulfur concentrations (1000—2000 ppm S; Hauff et al., 1997) in these fresh glasses from pillow rims indicate low degrees of degassing. Therefore, they likely erupted in moderate to deep water depths (Moore & Schilling, 1973). In most of the sites, the thickness of the cooling units (up to 50 m) and the paucity or lack of primary sediment intercalations suggests high eruption rates over relatively short time intervals, thus ensuring good preservation and little to no post-eruptive alteration of the volcanic deposits.

The ophiolitic complex is overlain in the north by Middle Campanian-Maastrichtian shallow-water carbonate deposits (e.g. Baumgartner-Mora & Denyer, 2002), and in the center by Albian black shales and Coniacian-Campanian pelagic to turbiditic sequences. The Murciélago Islands, north of the Nicoya Peninsula, are not considered part of the Santa Helena ophiolite located to the east, because the basalts are geochemically almost identical to the CLIP and the older basaltic suites of the Nicoya Peninsula (Escuder-Viruete et al., 2015; Madrigal et al., 2015).

Two sample collections were available for this study: the CR and NC collections (Table 1 and Figure 1). The CR collection consists of 10 sites of pillow rinds and hyaloclastites. Sites CR01-04 were collected from outcrops along the beach east of Playa del Coco and from the same tectonic block. In this study, we present new <sup>40</sup>Ar/<sup>39</sup>Ar dates from sites CR01 ( $131.0 \pm 3.2$  Ma) and CR03 ( $130.0 \pm 4.5$  Ma). Additional <sup>40</sup>Ar/<sup>39</sup>Ar ages are available from this area. We have recalculated them using consistent age standards and K decay constants (Fleck et al., 2019). These recalculated published ages include  $141.4 \pm 1.1$  Ma (originally  $139.1 \pm 1.1$  Ma; sample AN8 by Hoernle et al., 2004),

276  $139.9 \pm 1.8$  Ma (originally  $137.6 \pm 1.8$  Ma; sample AN10 by Hoernle et al., 2004) and  
 277  $136.5 \pm 2.5$  Ma (originally  $137.1 \pm 2.5$  Ma; sample NI7 by Madrigal et al., 2016). Thus,  
 278 we use a weighted mean age of  $140.99 \pm 0.94$  Ma (Mean Squares Weighted Deviation  
 279 (MSWD) = 2.0, Probability (P) = 15%, from close-proximity samples AN8 and AN10; Hoernle  
 280 et al., 2004) for the CR02 and CR04 sites. Sites CR05 and CR06 are from northeast of  
 281 Playa Hermosa, in the same location as the BN22 site dated at  $112.4 \pm 0.9$  Ma (orig-  
 282 inally  $110.6 \pm 0.9$  Ma; Hoernle et al., 2004). Samples CR13 and CR14 are from west-  
 283 ern Playa del Coco, both from the same pillow lava sequence dated at  $135.1 \pm 1.5$  Ma  
 284 (originally  $132.9 \pm 1.5$  Ma; sample AN3 by Hoernle et al., 2004). In the central-western  
 285 coast, site CR18 is dated at  $121.4 \pm 1.1$  Ma (originally  $119.4 \pm 1.1$  Ma; sample AN34  
 286 from Hoernle et al., 2004). Further south, site CR20 has a slightly younger age of  $120.2$   
 287  $\pm 1.8$  Ma (originally  $118.2 \pm 1.8$  Ma; sample AN40 from Hoernle et al., 2004). Sites NC17-  
 288 18 and NC19-28 from this study were collected at the same locations as CR18 and CR19-  
 289 CR20, respectively. The NC sample set (Figures 1 and 2) consists of 38 single pillow  
 290 basalts, where each pillow represents a sampling site. Fragments of fresh basaltic glass  
 291 were collected from pillow rinds (Table 1, Figures 1 and 2). The ages of the NC col-  
 292 lection were assigned using their close-proximity to dated sites from previous studies (Ta-  
 293 ble 1, Figure 1). From the north of the Nicoya Peninsula, in the Murciélago Islands, we  
 294 collected samples from five sites, NC01-05; NC01 and NC03-05 with a close-proximity  
 295  $^{40}\text{Ar}/^{39}\text{Ar}$  age of  $110.6 \pm 2.0$  Ma (originally  $109.0 \pm 2.0$  Ma; sample SE6 from Hauff et  
 296 al., 2000) and site NC02 with an age of  $113.0 \pm 3.5$  Ma (originally  $113.4 \pm 3.5$  Ma; sam-  
 297 ple SE-050611-11 from Madrigal et al., 2016). From north to south on the Nicoya Penin-  
 298 sula, 29 sites (NC06-34) were collected. Sites NC31-32 were dated at 94 Ma (based on  
 299 close-proximity to a radiolaria biostratigraphic age from site NB03; Tournon & Alvarado,  
 300 1997). Site NC33 was dated at  $96.1 \pm 0.9$  Ma (originally  $94.7 \pm 0.9$  Ma, based on nearby  
 301 site AN86 of Hauff et al., 2000) and finally from the south, at Quepos, sites NC36-38 were  
 302 dated at  $64.7 \pm 0.5$  Ma (originally  $63.9 \pm 0.5$  Ma, based on the close-proximity to sam-  
 303 ple S-QP93-1; Sinton et al., 1997).

#### 304 4 Methods and results

305 In this study, we analysed a total of 360 specimens from 42 sites using the IZZI method  
 306 of Yu et al. (2004). Tauxe and Staudigel (2004) used this method to study SBG sam-  
 307 ples from the Troodos Ophiolite in Cyprus. The IZZI protocol embeds two variations of  
 308 the Thellier-Thellier method: the in-field, zero-field (IZ) method of Aitken et al. (1988)  
 309 and the zero-field, in-field (ZI) method of Coe (1967) with the addition of the so-called  
 310 partial Thermal Remanent Magnetization (pTRM) checks of Coe et al. (1978). This ap-  
 311 proach ensures a built-in check for alteration during the experiments and a test of the  
 312 so-called ‘Reciprocity Law’ of Thellier and Thellier (1959).

313 Between 8 to 20 SBG specimens were analysed per site, following the suggestion  
 314 of Santos and Tauxe (2019) that if an experiment contains a sufficient number of spec-  
 315 imens, the field estimate is affected by a large bias. In this study, we performed 20 to  
 316 48 heating steps per experiment in four experiments with three different laboratory fields  
 317 (15, 25 and 45  $\mu\text{T}$ ).

318 Data were analysed using the PmagPy software package (Tauxe et al., 2016). The  
 319 Natural Remanent Magnetization (NRM) values remaining after each heating step were  
 320 plotted against the pTRM gained in Arai plots (Nagata et al., 1963) along with corre-  
 321 sponding Zijdeveld (Zijdeveld, 1967), equal area, magnetization versus temperature (M/T)  
 322 and site level plots (Figure 3). The criteria used in this study were used as threshold val-  
 323 ues to select the most reliable and straight Arai plots and were similar to the strict CCRIT  
 324 set of Cromwell et al. (2015) and Tauxe et al. (2016). Acceptable (successful) specimens  
 325 were characterized by three or more pTRM checks ( $N_{pTRM}$ ); a Fraction of Remanence  
 326 (FRAC) value used in the slope calculation (defined by Paterson et al. (2014)) of greater  
 327 than or equal to 0.78, SCAT (=True),  $b_{beta}$  value greater than 0.1, MAD and DANG

Site	Location	Type	Lat (°N)	Long (°W)	Age (Ma)	2 $\sigma$	Ref.
NC01	N of Isla San Pedrito	glassy pm	10.856	85.952	113.0	3.5	3
NC02	Golondrina Island	pm	10.856	85.944	113.0	3.5	3
NC03	San Jose Island	pm	10.854	85.926	113.0	3.5	3
NC04	Cocinera Island	SBG	10.857	85.907	110.6	2.0	2
NC05	San Jose Island	SBG	10.851	85.912	113.0	3.5	3
NC06	N of P. Guacamaya	SBG	10.533	85.781	[-]	[-]	[-]
NC07	P. Junquillal/ Hermosa	fine pm	10.154	85.808	[-]	[-]	[-]
NC08	P. Blanca	SBG	10.181	85.821	[-]	[-]	[-]
NC09A	Venado	SBG	10.128	85.798	[-]	[-]	[-]
NC09B	Venado	SBG	10.127	85.797	[-]	[-]	[-]
NC10A	La Joya del Lagarto	SBG	10.112	85.794	[-]	[-]	[-]
NC10B	La Joya del Lagarto	fine pm	10.112	85.795	[-]	[-]	[-]
NC11	Near NC10	SBG	10.108	85.794	[-]	[-]	[-]
NC12A	P. Nilo	pm	10.105	85.791	[-]	[-]	[-]
NC12B	P. Nilo	hyalo.	10.105	85.791	[-]	[-]	[-]
NC13	N of P. Pitahaya	SBG	10.067	85.77	[-]	[-]	[-]
NC14	between P. Nilo & P. Frijolar	hyalo.	10.095	85.789	[-]	[-]	[-]
NC15	near NC14	SBG	10.095	85.789	[-]	[-]	[-]
NC16	near NC15	SBG	10.093	85.787	[-]	[-]	[-]
NC17	San Juanillo	SBG	10.034	85.739	121.4	1.1	1
NC18	Punta Islita	SBG	9.85	85.404	121.4	1.1	1
NC19	Punta Islita	SBG	9.848	85.402	120.2	1.8	1
NC20	Punta Islita	SBG	9.848	85.403	[-]	[-]	[-]
NC21	Punta Islita	SBG	9.848	85.403	[-]	[-]	[-]
NC22	P. Corozalito	SBG	9.846	85.383	120.2	1.8	1
NC23	P. Corozalito	glassy pm	9.848	85.383	120.2	1.8	1
NC24	P. Corozalito	glassy pm	9.849	85.382	120.2	1.8	1
NC25	P. Corozalito	glassy pm	9.844	85.374	120.2	1.8	1
NC26	camping Corozalito	glassy pm	9.845	85.374	120.2	1.8	1
NC27	camping Corozalito	glassy pm	9.845	85.373	120.2	1.8	1
NC28	camping Corozalito	glassy pm	9.845	85.374	120.2	1.8	1
NC29	P. Bejuco		9.823	85.331	120.2	1.8	1
NC30	Punta coyote		9.76	85.275	[-]	[-]	[-]
NC31	P. Las Manchas	pm	9.644	85.073	94	[-]	5
NC32	P. Las Manchas		9.646	85.072	94	[-]	5
NC33	Ballena Bay		9.737	84.977	96.1	0.9	2
NC34	P. Posa Colorada	glassy pm	9.788	84.922	[-]	[-]	[-]
NC35	P. Los Muertos	glassy pm	9.76	84.893	[-]	[-]	[-]
NC36	P. Espadilla	weathered p.	9.389	84.148	64.7	0.5	4
NC37	P. Espadilla	p. breccia	9.388	84.147	64.7	0.5	4
NC38	P. Las Gemelas	fine grained	9.38	84.14	64.7	0.5	4
CR01	Punta Cacique	hyalo.	10.566	85.693	131.0	1.6	TS
CR02	Punta Cacique	glassy pm	10.569	85.7	141.0	0.9	1/TS
CR03	Punta Cacique	hyalo.	10.571	85.687	130.0	4.5	TS
CR04	Punta Cacique	hyalo.	10.569	85.685	141.0	0.9	1/TS
CR05	NE of P. Hermosa	glassy pm	10.589	85.68	112.4	0.9	1
CR06	near CR5	glass pm	10.588	85.679	112.4	0.9	1
CR13	Punta Miga	hyalo.	10.555	85.709	135.1	1.5	1
CR14	Punta Miga	glassy pm	10.55	85.707	135.1	1.5	1
CR18B	P. San Juanillo	glassy pm	10.029	85.739	121.4	1.1	1
CR20B	P. Corozalito	hyalo.	9.848	85.383	120.2	1.8	1

**Table 1.** Site, location name and coordinates. Abbreviations: pm=pillow margin; SBG= submarine basaltic glass; hyalo.= hyaloclastite; P= playa; Lat.= Latitude; Lon= Longitude; Ref.= Reference. The literature  $^{40}\text{Ar}/^{39}\text{Ar}$  ages were recalculated using the standard ages and K decay of Fleck et al. (2019). Reference 1= Hoernle et al., 2004; 2= Hauff et al., 2000; 3= Madrigal et al., 2016; 4= Sinton et al., 1997; 5= Tournon & Alvarado, 1997 (radiolaria biostratigraphic age); and TS= this study.



values of lower than or equal to 10, and a  $|k^{\vec{r}}|$  (the curvature value of Paterson, 2011, evaluated over the selected interval) of less than or equal to 0.164. For a few specimens with clear two component behavior in the directions, we allowed the FRAC value to be as low as 0.3 (CCRIT-relaxed), and used the slope of the line associated with the characteristic component. For a complete definition of the selection criteria we refer to the paper of Paterson et al. (2014). The selection criteria at site level required that the number of successful specimens per site ( $N_{spec.}$ ) was greater than 3 and the standard deviation was lower than  $10 \mu\text{T}$ .

#### 4.1 $^{40}\text{Ar}/^{39}\text{Ar}$ methods and results

$^{40}\text{Ar}/^{39}\text{Ar}$  dating was undertaken on two basaltic glass samples (CR01 and CR03) at the Argon Geochronology in Oceanography (ArGO) Laboratory at GEOMAR Helmholtz Centre of Ocean Research Kiel. A detailed description of the methods and equipment used can be found in Homrighausen et al. (2019) and the full data is presented in Tables DR1 and DR2 (Supplementary material). The samples were irradiated for 168 hours at 5 MW, in the C6 position of the GKSS nuclear reactor, Germany. Aliquots of the Taylor Creek sanidine age standard (TCs;  $28.344 \pm 0.011 \text{ Ma}$  ( $1\sigma$ ; Fleck et al., 2019) were co-irradiated with the unknown samples, and the  $K(\text{total})$  decay constant of Steiger and Jäger (1977) was used. In order to robustly compare our new data with the literature's  $^{40}\text{Ar}/^{39}\text{Ar}$  ages, the ages of Sinton et al. (1997), Hauff et al. (2000), Hoernle et al. (2004), and Madrigal et al. (2016) were recalculated utilizing the ArAR calculator of Mercer and Hodges (2016), using the total  $^{40}\text{K}(\text{total})$  decay constant of Steiger and Jäger (1977), as per the recommendation of Fleck et al. (2019). The following standard ages were also applied to the previously published  $^{40}\text{Ar}/^{39}\text{Ar}$  data: a TCs age of  $28.344 \pm 0.011 \text{ Ma}$  ( $1\sigma$ ; Fleck et al., 2019) to the data of Hauff et al. (2000) and Hoernle et al. (2004) data, a Fish Canyon sanidine age of  $28.099 \pm 0.013 \text{ Ma}$  (FCs; ( $1\sigma$ ; Fleck et al., 2019) to the Madrigal et al. (2015) data, and a Fish Canyon Tuff biotite age of  $28.06 \text{ Ma}$  (FCT-3; Kuiper, Deino, & Hilgen, 2008) was applied to the Sinton et al. (1997) data. The recalculated  $^{40}\text{Ar}/^{39}\text{Ar}$  ages are quoted Figure 1 in Tables 1-2.  $^{40}\text{Ar}/^{39}\text{Ar}$  dating of samples CR01 and CR03 yielded plateau ages of  $131.0 \pm 3.2 \text{ Ma}$  (61.0%  $^{39}\text{Ar}$ ; MSWD = 0.41,  $P = 93\%$ ) and  $130.0 \pm 4.5 \text{ Ma}$  (67.8%  $^{39}\text{Ar}$ ; MSWD = 0.41,  $P = 96\%$ ), respectively. Both age spectra are disturbed, and high Cl concentrations (monitored by the analysis of the mass 35.5 baseline value) were observed in many steps. Initial step-heating analyses yielded very high quantities of atmospheric  $^{40}\text{Ar}$ , and overall both samples show quite high atmospheric  $^{40}\text{Ar}$  concentrations of 26-99% (CR01) and 35-99% (CR03), which suggests that the basaltic glass samples may have been affected by alteration. These factors may explain the large age uncertainties observed in some steps of both samples (Table DR2). Inverse isochrons plots from the plateau steps of each sample yielded isochron ages within  $2\sigma$  uncertainties of the plateau ages:  $130 \pm 11 \text{ Ma}$  (CR01; 95% confidence (95% conf.); MSWD = 0.48,  $P = 87$ , with an unacceptable Spreading Factor (SF) value of 25.1%), and  $136 \pm 11 \text{ Ma}$  (CR03; 95% conf.; MSWD = 0.33;  $P = 98\%$ , with an acceptable SF value of 41.0%). Both samples yielded initial  $^{40}\text{Ar}/^{36}\text{Ar}$  ratios of  $297 \pm 12$  (CR01) and  $288 \pm 13$  (CR03), within 95% conf. uncertainties of the atmospheric  $^{40}\text{Ar}/^{36}\text{Ar}$  ratio of 295.5 (Steiger & Jäger, 1977; Tables DR1 and DR2, Supplementary material).

#### 4.2 Paleointensity results

Overall, 21 of the 360 specimens and 4 of the 42 sites analysed passed the strict selection criteria (CCRIT-strict, Table 2), while 69 of 360 specimens and nine of the 42 sites passed the modified CCRIT (Paterson et al., 2014) (CCRIT-relaxed, with a FRAC greater than 0.3; Table 2), with an overall 6 and 20% success rate at the specimen level.

The main reason for failure (77% of specimens) was a combination of criteria which together indicated alteration of the sample, as shown by failed pTRM checks, segmented or curved Arai plots (e.g. Figure 3b) suggesting the presence of multidomain-like grains

379 and random and chaotic behavior (30.5%). 12% of the specimens failed the FRAC cri-  
 380 terion because of the presence of multi-components of the remanent magnetization (e.g.,  
 381 Figure 3d). A further 11% failed because of  $k'$ , thought to reflect a threshold separ-  
 382 ating single-domain-like from multidomain-like remanences. In case of evidence of multi-  
 383 multiple components of remanent magnetization observed on some of the Zijderveld diagrams  
 384 (for instance, Figure 3c; Zijderveld, 1967), we selected only the temperature steps cor-  
 385 responding to the characteristic remanent magnetization (ChRM) component heading  
 386 towards the origin of the Zijderveld. For these specimens, we relaxed the FRAC crite-  
 387 rion to 0.3. For instance, Figure 3d shows a Zijderveld diagram that clearly indicates two  
 388 components, a low temperature (NRM to 300°C) and the ChRM from 350 to 495°C head-  
 389 ing towards the origin. Overall, the NRM values vary significantly from about 5.3  $\mu\text{Am}^2$   
 390 to 30  $\mu\text{Am}^2$  and the intensities vary from 21  $\mu\text{T}$  to 37  $\mu\text{T}$  (Table 2).

391 The swarm-violin plot (Figure 4a) shows the distribution of all specimens which  
 392 passed the CCRIT-relaxed selection criteria at the specimen level (Table 2). Of the four-  
 393 teen sites, only three (CR03, CR18, and NC01) have two or three specimens. Specimens  
 394 from three sites (CR01, CR06 and CR14) show a high dispersion distribution. The re-  
 395 maining eight sites (CR02, CR05, CR06, NC02, NC03 and NC17) show a low dispersion  
 396 of the density distribution, are symmetric around their mean values and are the only spec-  
 397 imens passing the CCRIT-relaxed site level selection criteria. When the strictest CCRIT-  
 398 strict criteria are applied (Table 2 and Figure 4b), three sites are characterised by only  
 399 two specimens, (CR02, CR03 and NC03) while sites CR13 and CR20 shows a high dis-  
 400 persion distribution and a  $\sigma\%$  greater than 25%, thus they do not pass the strict selec-  
 401 tion criteria. Finally, site CR14 is characterized by a  $\sigma\%$  of 23%, thus it can be consid-  
 402 ered reliable.

Site	Age (Ma)	n/N	B ( $\mu\text{T}$ )	$\sigma$ (%)	Lat ( $^\circ\text{N}$ )	VADM	VADM1
<i>strict</i>							
CR06	112.4 $\pm$ 0.9	7/24	33.7 $\pm$ 3.9	11.6	3.6	86.6 $\pm$ 10.0	83.0 $\pm$ 9.6
CR05	112.4 $\pm$ 0.9	6/18	20.7 $\pm$ 3.2	15.6	3.6	53.2 $\pm$ 8.2	51.0 $\pm$ 7.8
NC17	121.4 $\pm$ 1.1	3/8	21.3 $\pm$ 1.2	5.6	9.5	53.0 $\pm$ 3.0	52.8 $\pm$ 3.0
CR14	135.1 $\pm$ 1.5	5/24	34.4 $\pm$ 8.1	23.0	3.6	88.4 $\pm$ 20.0	84.8 $\pm$ 19.9
<i>relaxed</i>							
CR06	112.4 $\pm$ 0.9	13/24	32.9 $\pm$ 3.8	11.6	3.6	84.6 $\pm$ 9.7	81.1 $\pm$ 9.4
CR05	112.4 $\pm$ 0.9	16/18	20.37 $\pm$ 5.0	23.8	3.6	52.2 $\pm$ 12.6	50.0 $\pm$ 12.3
NC02	113.0 $\pm$ 3.5	6/17	29.0 $\pm$ 7.0	24.2	1.5	74.9 $\pm$ 18.1	71.3 $\pm$ 17.2
NC03	113.0 $\pm$ 3.5	9/18	37.4 $\pm$ 7.4	19.6	1.5	96.6 $\pm$ 19.1	91.9 $\pm$ 18.1
NC17	121.4 $\pm$ 1.1	6/8	21.8 $\pm$ 5.9	26.9	9.5	54.2 $\pm$ 14.6	54.0 $\pm$ 14.6
CR18	121.4 $\pm$ 1.1	3/10	32.3 $\pm$ 3.2	9.8	9.5	80.4 $\pm$ 8.0	80.0 $\pm$ 7.9
CR03	130.0 $\pm$ 4.5	3/12	32.3 $\pm$ 0.6	1.9	3.6	83.0 $\pm$ 1.5	79.6 $\pm$ 1.5
CR14	135.1 $\pm$ 1.5	12/24	32.9 $\pm$ 7.3	22.3	3.6	84.6 $\pm$ 18.7	81.1 $\pm$ 17.9
CR02	141.0 $\pm$ 0.9	4/6	21.4 $\pm$ 2.0	3.6	3.6	55.0 $\pm$ 5.4	52.7 $\pm$ 5.1

**Table 2.** Paleointensity results from Costa Rica obtained with the CCRIT-strict selection criteria, and CCRIT-relaxed with a FRAC value greater than 0.3. The  $^{40}\text{Ar}/^{39}\text{Ar}$  ages are shown with  $2\sigma$  uncertainties). Abbreviations: n/N = number (n) of specimens yielding a reliable paleointensity signal and total number of specimens analysed (N), B = paleointensity values. Lat ( $^\circ\text{N}$ )= paleolatitude reported by Boshman et al. (2019), VADM and VADM1 = Virtual Axial Dipole Moment values ( $\text{ZAm}^2=10^{21} \text{Am}^2$ ) calculated using the Boshman et al. (2019) paleolatitudes and present day latitudes, respectively. Sites for which no paleointensity could be obtained are omitted from this table.

At the site level (Figure 5), intensities before the onset of the CNS ( $\sim 141$  Ma) are low and similar to the values around the onset of the CNS ( $\sim 121$ , sites NC17 and CR02). After the onset of the CNS the intensity values vary between  $20 \pm 4 \mu\text{T}$  (site CR05) and  $37 \pm 7 \mu\text{T}$  (site NC03), with an average of  $29 \pm 7 \mu\text{T}$ .

## 5 Discussion

In total, reliable paleointensity estimates have been obtained for four sites from Costa Rica, with ages spanning a 23 Ma interval between 135 and 112 Ma, using the CCRIT-strict selection criteria and nine sites spanning 145 to 112 Ma using the CCRIT-relaxed criteria (Table 2, Figure 5). Of the successful sites passing the CCRIT-strict criteria (Table 2), two are from the early CNS (112 Ma), one is close to the CNS onset (121 Ma) and one is from the pre-CNS (135 Ma). Of the successful sites passing the CCRIT-relaxed criteria (Table 2), three are from the pre-CNS (145-130 Ma), two are close to the CNS onset (121 Ma) and four are from the early CNS (113-112 Ma). In order to compare our results from Costa Rica to all the other data from similar ages, we calculated the virtual axial dipole moments (VADMs), using both paleolatitudes from the study of Boshman et al. (2019) (VADM; Table 2 and Figure 5) and the present-day latitude (VADM1; Table 2 and Figure 5), between  $9$  and  $10^\circ$  N (Table 1). The paleolatitudes reported by Boshman et al. (2019) range between  $1$  and  $9^\circ$  N (Table 2). These VADMs values are systematically slightly higher than the VADM1s values, but statistically indistinguishable (overlapping within the quoted  $1\sigma$  errors). When we consider our results obtained with the CCRIT-strict criteria, one site with an age of 135 Ma gives reliable intensity results of  $34 \pm 8 \mu\text{T}$  (equivalent to a paleomagnetic dipole moment, PDM, of  $88 \pm 20 \text{ZAm}^2$ ), while one site with an age of 121 Ma gives a value of  $21 \pm 1 \mu\text{T}$  (or  $53 \pm 3 \text{ZAm}^2$  during the onset of the CNS and two sites with ages of 112 give variable intensity values ranging from  $21 \pm 3$  to  $34 \pm 4 \mu\text{T}$  (or  $53 \pm 8$  to  $87 \pm 10 \text{ZAm}^2$ ) after the onset of the CNS. Considering the results obtained with the CCRIT-relaxed criteria, the average paleointensity value from Costa Rica during the CNS is  $\sim 29 \mu\text{T}$  ( $\sim 77 \text{ZAm}^2$ ), whereas the pre-CNS records a lower intensity value of  $21 \pm 1 \mu\text{T}$  (or VADM of  $53 \pm 3 \text{ZAm}^2$ ). Unfortunately, the recognition of any trend is limited by the lack of data between 135-121 and 121-112 Ma, around the onset of the CNS.

In order to verify the polarity and the reliability of the close-proximity geochronological ages assigned to our sites, (CNS sites are expected to have normal polarities), we tried to compare the directional data of Boshman et al. (2019), which were obtained from the same locations as this study. Unfortunately, our sampling did not include drilling oriented core samples. In addition, all of Boshman et al. (2019) sites (except for a few that failed a fold test) are interpreted as having normal polarity, including the sampling site near our CR14 site, which was  $^{40}\text{Ar}/^{39}\text{Ar}$  dated at  $135.1 \pm 1.5$  Ma (Hoernle et al., 2004). Therefore, the directional information by Boshman et al. (2019) cannot provide a test of the  $^{40}\text{Ar}/^{39}\text{Ar}$  ages. Data from this study (shown as red and black stars, for results obtained using the CCRIT-strict and CCRIT-relaxed, respectively, in Figure 6) display similar to lower values than the present-day field (red dashed line in Figure 6, calculated using the International Geomagnetic Reference Field (IGRF) model, and equal to or slightly higher than the average value of  $50 \text{ZAm}^2$  previously obtained for the CNS (blue solid line in Figure 6, Bol'shakov & Solodnikov, 1983; Pick & Tauxe, 1993a; Zhu et al., 2001; Zhu, Hoffman, et al., 2004). In order to compare the new paleointensity data from Costa Rica with the existing database, we adopted a consistent approach. We re-analysed the available data using the same set of CCRIT-relaxed criteria, as employed in this study. Only five studies published the original measurement data, following the FAIR, or Findability, Accessibility, Interoperability and Reusability, principles (Wilkinson et al., 2016). After our re-analyses, fewer sites were found to pass the CCRIT-relaxed selection criteria compared to the results of the original studies. From the study of Zhu et al., 2008, 73% (25 of 34) of the original sites pass CCRIT-relaxed criteria. In the study

of Tauxe and Staudigel (2004), only 23% (9 of 39) of the sites pass. In Figure 6, we plot all the available data for the last 200 Ma from the MagIC database as grey circles, and the reinterpreted data from literature as orange, green, pink, blue and purple circles (Tauxe & Staudigel, 2004; Granot et al., 2007; Zhu et al., 2008; Tauxe et al., 2013; Tauxe, 2006), respectively. The Costa Rica paleointensity values are similar to the 114-110 Ma Sohongtu values obtained by Zhu et al. (2008) and to the re-interpreted late-CNS mean values obtained for the late CNS after re-interpreting the data from the SBG Troodos ophiolite (92 Ma; Tauxe and Staudigel 2004; Granot et al., 2007). Indeed, we obtained average re-calculated values of 65.4 ZAm<sup>2</sup> (Tauxe & Staudigel, 2004) and 55.9 ZAm<sup>2</sup> (Granot et al., 2007)(orange and green circles in Figure 6).

The average Costa Rica paleointensity values is  $\sim 13$  ZAm<sup>2</sup> higher than the values of the long-term average of 42 ZAm<sup>2</sup> suggested by Juarez et al. (1998) but is similar to the mean value of  $\sim 50$  ZAm<sup>2</sup> calculated using the entire MagIC database from the last 200 Ma. These results appear to contradict the suggestion by Selkin and Tauxe (2000) that the distribution of paleointensities does not change substantially between 124 and 30 Ma (low reversal rate) and 30-0.3 Ma (high reversal rate). At the same time, our data do not seem to support the hypothesis that long periods of low reversal frequency are characterized by a stronger field than periods of high reversal rates (Tauxe & Hartl, 1997; Constable et al., 1998). It is worth noticing that the re-analysis of SBG samples from DSDP and ODP drill cores compiled by Tauxe (2006) from 0 to 122 Ma suggests a consistently weaker field than previously reported and provide low values at both the onset and toward the end of the CNS. Together, Costa Rica and the Troodos ophiolite data show a relatively weak field just before the onset of the CNS (around 121 Ma) but a stronger field both during the first 20 Ma and towards the end of the CNS. The paucity of data between 110 and 95 Ma hampers the interpretation of any paleointensity field trend during the middle part of the CNS.

Monte Carlo simulations, using the TK03 paleosecular variation model of Tauxe and Kent (2004), show that at least 25 estimates for a given age are required to robustly estimate paleofield strength value (Tauxe & Staudigel, 2004). Unfortunately, none of the individual studies available so far have sufficient temporal sampling to provide a robust estimate of the paleofield strength during the CNS.

Indeed, a robust record of reversals and excursions is needed, along with a reliable and temporally and spatially well distributed paleointensity dataset in order to verify a possible correlation between dipole strength and reversal frequency. This in turn, would provide important constraints on the heat flux across the Earth's core-mantle boundary, the energy states of the geodynamo and their modelling (Biggin et al., 2012). The new, reliable and robust paleointensity data from Costa Rica contribute significantly to the current dataset and can be used in future numerical simulations in order to understand long-term variations, the geomagnetic field features and whether these are a result of external forcing mechanisms and/or reflect the hydrodynamic processes occurring in the Earth's mantle, outer core and inner core.

## 6 Conclusions

This study provides high-quality paleointensity data from 13 sites Costa Rica, spanning 23 Ma of volcanic activity, between 135 and 112 Ma, from before the onset of the CNS and during the beginning of the CNS.

- We investigated 42 submarine basaltic glass (SBG) sites from pillow lava margins, sampled along the coast from the upper crust sequences of the Murciélago Islands and Nicoya ophiolite, from the north, north-west, and the south of the Nicoya Peninsula.

- 504 • New  $^{40}\text{Ar}/^{39}\text{Ar}$  ages are presented, and, along with  $^{40}\text{Ar}/^{39}\text{Ar}$  and biostratigraphic  
505 ages from previous studies, indicate ages ranging from 141 to 94 Ma.
- 506 • We present new high-quality paleointensity results from four sites, with ages from  
507 135 to 112 Ma, obtained using the IZZI protocol and applying a CCRIT-strict se-  
508 lection criteria.
- 509 • Allowing interpretation of two-component magnetization by relaxing the FRAC  
510 criterion (CCRIT-relaxed) resulted in the inclusion of an additional nine sites with  
511 ages from 141 Ma to 112 Ma.
- 512 • The new paleointensity data from before the onset of the CNS (135 Ma) yield a  
513 value of  $34 \pm 8 \mu\text{T}$  (or a PDM value of  $88 \pm 20 \text{ZAm}^2$ ), one paleointensity value  
514 for the onset of the CNS at 121 Ma ( $21 \pm 1 \mu\text{T}$  or  $53 \pm 3 \text{ZAm}^2$ ), and two pa-  
515 leointensity values from the first part of the CNS vary from  $21 \pm 3$  to  $34 \pm 4 \mu\text{T}$   
516 (or  $53 \pm 8$  to  $87 \pm 10 \text{ZAm}^2$ ).
- 517 • These new CNS paleointensity results from Costa Rica are similar to the values  
518 from the 114-110 Ma Suhongtu lava section, Inner Mongolia, of  $\sim 50 \text{ZAm}^2$  (Zhu  
519 et al., 2008) and the  $\sim 92$  Ma Troodos Ophiolite, re-interpreted using the same strict  
520 criteria as in this study, of  $\sim 55 \text{ZAm}^2$  (Granot et al., 2007), but are lower than  
521 the Troodos Ophiolite paleointensity value of  $\sim 65 \text{ZAm}^2$  by Tauxe and Staudigel  
522 (2004).
- 523 • The new Costa Rica data indicate that the strength of the geomagnetic field was  
524 relatively lower during the onset of the CNS and higher in the early CNS, but all  
525 these values are higher than the average geomagnetic field strength. Finally, our  
526 data do not seem to support a correlation between the strength and stability of  
527 the geomagnetic field.
- 528 • These new paleointensity results can contribute to understanding long-term vari-  
529 ation and features of the Earth's Magnetic Field.

### 530 Acknowledgments

531 Data will be made available on the MagIC database: <https://earthref.org/MagIC/16870/d197f16c-70ef-459a-98c1-f8f67f757731>. This work was supported in part by NSF Grant EAR1547263  
532 to LT, and NEXT Data grant to FF and ADC. KH received funds from the GEOMAR  
533 Research Center. We thank Jan Sticklus for his help with the  $^{40}\text{Ar}/^{39}\text{Ar}$  dating of sam-  
534 ples at GEOMAR Helmholtz Centre for Ocean Research Kiel.  
535

### 536 References

- 537 Aitken, M. J., Allsop, A. L., Bussell, G. D., & Winter, M. B. (1988). Determina-  
538 tion of the intensity of the Earth's magnetic field during archeological times:  
539 reliability of the Thellier technique. *Rev. Geophys.*, *26*, 3–12.
- 540 Azema, J., Tournon, J., & Sornay, J. (n.d.). Presencia de amonites del Albiano  
541 Superior en las formaciones del Complejo de Nicoya. El yacimiento de Loma  
542 Chumico, provincia de Guanacaste, Costa Rica, volume = 2, year = 1978. *Inf.*  
543 *Sem. IGN*, 71–76.
- 544 Bandini, A. N., Flores, K., Baumgartner, P., Jackett, S. J., & Denyer, P. (2008).  
545 Late Cretaceous and Paleogene radiolaria from the Nicoya Peninsula, Costa  
546 Rica: a tectonostratigraphic application. *Stratigraphy*, *5*, 3-21.
- 547 Baumgartner, P. (1984). El complejo ofiolítico (Costa Rica): Modelos estruc-  
548 turales analizados en función de las edades de los Radiolarios (Calloviense  
549 a Santoniense). In: Spechmann, P., Ed. Manual de Geológico de Nicoya  
550 (Costa Rica): Modelos estructurales analizados en función de las edades de los  
551 Radiolarios (Calloviense a Santoniense). In: Spechmann, P., Ed. *Manual de*  
552 *Geología de Costa Rica, Universidad de Costa Rica*, 115-123.
- 553 Baumgartner, P., O'Dogherty, L., Goričan, Š., Urquhart, E., Pillevuit, A., &

- 554 De Wever, P. (1995). Middle Jurassic to Lower Cretaceous radiolaria of  
 555 Tethys: occurrences, systematics, biochronology.
- 556 Baumgartner-Mora, C., & Denyer, P. (2002). Campanian-Maastrichtian limestone  
 557 with larger foraminifera from Peñruja Rock (Santa Elena Peninsula). *Revista*  
 558 *Geológica Central*, *26*, 85-89.
- 559 Biggin, A., & McCormack, A., A. and Roberts. (2010). Paleointensity database up-  
 560 dated and upgraded. *Eos, Transactions American Geophysical Union*, *91*(2),  
 561 15–15.
- 562 Biggin, A., Steinberger, B., Aubert, J., Suttie, N., Holme, R., Torsvik, T. H., ... van  
 563 Hinsbergen, D. (2012). Possible links between long-term geomagnetic varia-  
 564 tions and whole-mantle convection processes. *Nature Geoscience*, *5*, 526-533.
- 565 Biggin, A., & Thomas, D. N. (2003). Analysis of long-term variations in the ge-  
 566 omagnetic poloidal field intensity and evaluation of their relationship with  
 567 global geodynamics. *Geophys. J. Int.*, *152*(2), 392-415.
- 568 Bol'shakov, A., & Solodnikov, G. M. (1983). Geomagnetic field intensity in Ar-  
 569 menia in the Late Jurassic and Early Cretaceous. *Izv. Earth Physics*, *19*, 976-  
 570 982.
- 571 Boshman, L., van der Wiel, E., Flores, K., Langereis, C., & van Hinsbergen, D.  
 572 (2019). The Caribbean and Farallon plates connected: Constraints from  
 573 stratigraphy and paleomagnetism of the Nicoya Peninsula, Costa Rica. *J.*  
 574 *Geophys. Res.-Solid Earth*, *123*, 6243-6266. doi: 10.1029/2018JB016369
- 575 Bowles, J., Gee, J. S., Burgess, K., & Cooper, R. F. (2011). Timing of magnetite  
 576 formation in basaltic glass: Insights from synthetic analogs and relevance for  
 577 geomagnetic paleointensity analyses. *Geochem. Geophys. Geosys.*, *12*(2).
- 578 Bowles, J., Gee, J. S., Kent, D., Bergmanis, E., & Sinton, J. (2005). Cooling  
 579 rate effects on paleointensity estimates in submarine basaltic glass and im-  
 580 plications for dating young flows. *Geochem. Geophys. Geosys.*, *6*, Q07002,  
 581 doi:10.1029/2004GC000900.
- 582 Brown, M., Korte, M., Holme, R., Wardinski, I., & Gunnarson, S. (2018). Earth's  
 583 magnetic field is probably not reversing. *Proc. Nat. Acad. Sci.*, *115*, 5111-5116.  
 584 doi: 10.1073/pnas.1722110115
- 585 Carlut, J., & Kent, D. (2000). Paleointensity record in zero-age submarine basalt  
 586 glass: Testing a new dating technique for recent MORBS. *Earth Planet. Sci.*  
 587 *Lett.*, *183*, 389-401.
- 588 Cejudo Ruiz, R., Goguitchaichvili, A., Morales, J., Trindade, R., Alva Valdivia, L.,  
 589 & Urrutia-Fucugauchi, J. (2009). Absolute Thellier paleointensities from Ponta  
 590 Grossa dikes (southern Brazil) and the early Cretaceous geomagnetic field  
 591 strength. *Geof. Int.*, *48*, 243-252.
- 592 Channell, J., Singer, B., & Jicha, B. (2020). Timing of Quaternary geomagnetic  
 593 reversals and excursions in volcanic and sedimentary archives. *Quat. Sci. Rev.*,  
 594 *228*. doi: 10.1016/j.quascirev.2019.106114
- 595 Coe, R. S. (1967). The determination of paleo-intensities of the Earth's magnetic  
 596 field with emphasis on mechanisms which could cause non-ideal behavior in  
 597 Thellier's method. *J. Geomag. Geoelectr.*, *19*, 157–178.
- 598 Coe, R. S., Grommé, S., & Mankinen, E. A. (1978). Geomagnetic paleointensities  
 599 from radiocarbon-dated lava flows on Hawaii and the question of the Pacific  
 600 nondipole low. *J. Geophys. Res.*, *83*, 1740–1756.
- 601 Constable, C. G., Tauxe, L., & Parker, R. L. (1998). Analysis of 11 Myr of geomag-  
 602 netic intensity variation. *J. Geophys. Res.-Solid Earth*, *103*(B8), 17735-17748.
- 603 Cottrell, R. D., & Tarduno, J. (2000). In search of high-fidelity geomagnetic paleoin-  
 604 tensities: A comparison of single plagioclase crystal and whole rock Thellier-  
 605 Thellier analyses. *J. Geophys. Res.*, *105*, 23579-23594.
- 606 Courtillot, V., Gallet, Y., Le Mouél, J.-L., Futeau, F., & Genevey, A. (2007). Are  
 607 there connections between the Earth's magnetic field and climate? *Earth*  
 608 *Planet. Sci. Lett.*, *253*(328-339).

- 609 Cox, A. V. (1968). Lengths of geomagnetic polarity intervals. *J. Geophys. Res.*, *73*,  
610 3247–3260.
- 611 Cromwell, G., Tauxe, L., & Halldórsson, S. (2015). New paleointensity results  
612 from rapidly cooled Icelandic lavas: Implications for Arctic geomagnetic field  
613 strength. *Journal of Geophysical Research: Solid Earth*, *120*(5), 2913–2934.
- 614 Cronin, M., Tauxe, L., Constable, C., Selkin, P., & Pick, T. (2001). Noise in the  
615 quiet zone. *Earth Planet. Sci. Lett.*, *190*, 13–30.
- 616 DeMets, C. (2001). A new estimate for present-day Cocos-Caribbean plate motion:  
617 Implications for slip along the Central American volcanic arc. *Geophys. Res.*  
618 *Lett.*, *28*, 4043–4046. doi: 10.1029/2001GL013518
- 619 Denyer, P., & Baumgartner, P. (2006). Emplacement of Jurassic-Lower Cretaceous  
620 radiolarites of the Nicoya Complex (Costa Rica). *Geologica Acta*, *4*, 203–218.
- 621 Denyer, P., & Gazel, E. (2009). The Costa Rican Jurassic to Miocene oceanic com-  
622 plexes: origin, tectonics and relations. *J. South Amer. Earth Sci.*, *28*, 429–442.
- 623 Dodd, S., Mac Niocaill, C., & Muxworthy, A. (2015). Long duration (>4 Ma) and  
624 steady-state volcanic activity in the early Cretaceous Paraná-Etendeka Large  
625 Igneous Province: New paleomagnetic data from Namibia. *Earth Planet. Sci.*  
626 *Lett.*, *414*, 16–29. doi: 10.1016/j.epsl.2015.01.009
- 627 Escuder-Viruete, J., Baumgartner, P. O., & Castillo-Carrión, M. (2015). Com-  
628 positional diversity in peridotites as result of a multi-process history: The  
629 Pacific-derived Santa Elena ophiolite, northwest Costa Rica. *Lithos*, *231*,  
630 16–34.
- 631 Fleck, R. J., Calvert, A. T., Coble, M. A., Wooden, J. L., Hodges, K., Hayden,  
632 L. A., ... John, D. A. (2019). Characterization of the rhyolite of Bodie Hills  
633 and  $^{40}\text{Ar}/^{39}\text{Ar}$  intercalibration with Ar mineral standards. *Chemical Geology*,  
634 *525*, 282–302.
- 635 Gallet, Y., & Hulot, G. (1997). Stationary and non-stationary behaviour within the  
636 geomagnetic polarity time scale. *Geophys. Res. Lett.*, *24*, 1875–1878.
- 637 Gee, J. S., & Kent, D. V. (2007). Source of oceanic magnetic anomalies and the geo-  
638 magnetic polarity timescale. In M. Kono (Ed.), *Geomagnetism* (Vol. 5, p. 455-  
639 507). Elsevier.
- 640 Glazmaier, G. A., Coe, R. S., Hongre, L., & Roberts, P. H. (1999). How the Earth’s  
641 mantle controls the frequency of geomagnetic reversals.
- 642 Gogutchachvili, A., Cejudo Ruiz, R., Sanchez-Bettucci, L., Reyes, B., Valdivia,  
643 L. M. A., Urrutia-Fucugauchi, J., ... Calvo-Rathert, M. (2008). New absolute  
644 paleointensity results from the Parana Magmatic Province (Uruguay) and the  
645 Early Cretaceous geomagnetic paleofield. *Geochem. Cosmochem. Acta.*, *9*. doi:  
646 10.1029/2008GC002102
- 647 Granot, R., Dymont, J., & Gallet, Y. (2012). Geomagnetic field variability during  
648 the Cretaceous Normal Superchron. *Nature Geoscience*, *5*, 220–223.
- 649 Granot, R., Tauxe, L., Gee, J., & Ron, H. (2007). A view into the Cretaceous ge-  
650 omagnetic field from analysis of gabbros and submarine glasses. *Earth Planet.*  
651 *Sci. Lett.*, *256*, 1–11. doi: 10.1016/j.epsl.2006.12.028
- 652 Gubbins, D. (1999). The distinction between geomagnetic excursions and reversals.  
653 *Geophys. J. Int.*, *137*, F1–F3.
- 654 Hauff, F., Hoernle, K., van den Bogaard, P., Alvarado, G., & Garbe-Schönberg.  
655 (2000). Age and geochemistry of basaltic complexes in western Costa Rica:  
656 Contributions to the geotectonic evolution of Central America. *Geochem.*  
657 *Geophys. Geosys.*, *1*, doi:10.1029/1999GC000020.
- 658 Heller, R., Merrill, R. T., & McFadden, P. L. (2002). The variation of intensity of  
659 earth’s magnetic field with time. *Phys. Earth Planet. Int.*, *131*(3–4), 237–249.
- 660 Helsley, C. E., & Steiner, M. B. (1968). Evidence for long intervals of normal polar-  
661 ity during the Cretaceous period. *Earth Planet. Sci. Lett.*, *5*, 325–332.
- 662 Hoernle, K., Hauff, F., & van den Bogaard, P. (2004). 70 m.y. history (139–69 Ma)  
663 for the Caribbean large igneous province. *Geology*, *32*, doi: 10.1130/G20574.1,

- 664 697-700.
- 665 Homrighausen, S., Hoernle, K., Hauff, F., Wartho, J.-A., van den Bogaard, P., &  
666 Garbe-Schönberg, D. (2019). New age and geochemical data from the Walvis  
667 Ridge: The temporal and spatial diversity of South Atlantic intraplate volcan-  
668 ism and its possible origin. *Geochimica et Cosmochimica Acta*, *245*, 16–34.
- 669 Hulot, G., Eymin, C., Langlais, B., Manda, M., & Olsen, N. (2002). Small-scale  
670 structure of the geodynamo inferred from Oersted and Magsat satellite data.  
671 *Nature*, *416*, 620-623.
- 672 Hulot, G., & Gallet, Y. (2003). Do superchrons occur without any paleomagnetic  
673 warning? *Earth Planet. Sci. Lett.*, *210*, 191-201. doi: 10.1016/S0012-821X(03)  
674 00130-4
- 675 Ingham, E., Heslop, D., Roberts, A. P., Hawkins, R., & Sambridge, M. (2014).  
676 Is there a link between geomagnetic reversal frequency and paleointen-  
677 sity? A Bayesian approach. *J. Geophys. Res.*, *119*, 5290-5304. doi:  
678 10.1002/2014JB010947
- 679 Juarez, M., & Tauxe, L. (2000). The intensity of the time averaged geomagnetic  
680 field: the last 5 m.y. *Earth Planet. Sci. Lett.*, *175*, 169-180.
- 681 Juarez, M., Tauxe, L., Gee, J. S., & Pick, T. (1998). The intensity of the Earth's  
682 magnetic field over the past 160 million years. *Nature*, *394*, 878-881.
- 683 Kent, D. V., & Gee, J. (1996). Magnetic alteration of zero-age oceanic basalt. *Geol-*  
684 *ogy*, *24*, 703-706.
- 685 Kuiper, K., Deino, A., & Hilgen, F. (2008). others, 2008. *Synchronizing rock clocks*  
686 *of Earth history: Science*, *320*, 500–504.
- 687 Kulakov, E., Sprain, C., Doubrovine, P., Smirnov, A., Paterson, G., Hawkins, L.,  
688 ... Biggin, A. (2019). Analysis of an Updated Paleointensity Database (QPI-  
689 PINT) for 65–200 Ma: Implications for the Long-Term History of Dipole Mo-  
690 ment Through the Mesozoic. *J. Geophys. Res.-Solid Earth*, *124*, 9999-10022.  
691 doi: 10.1029/2018JB017287
- 692 Larson, R. L., & Olson, P. (1991). Mantle plumes control magnetic reversal fre-  
693 quency. *Earth Planet. Sci. Lett.*, *107*, 437–447.
- 694 Loper, D. E., & McCartney, K. (1986). Mantle plumes and the periodicity of mag-  
695 netic field reversals. *Geophys. Res. Lett.*, *13*, 1525–1528.
- 696 Madrigal, P., Gazel, E., Denyer, P., Smith, I., Jicha, B., Flores, K., ... Snow,  
697 J. (2015). A melt-focusing zone in the lithospheric mantle preserved  
698 in the Santa Elena Ophiolite, Costa Rica. *Lithos*, *230*, 189-205. doi:  
699 10.1016/j.lithos.2015.04.015
- 700 Madrigal, P., Gazel, E., Flores, K., Bizimis, M., & Jicha, B. (2016). Record of mas-  
701 sive upwellings from the Pacific large low shear velocity province. *Nature Com-*  
702 *munications*, *7*(13309). doi: 10.1038/ncomms13309
- 703 McElhinny, M., & Larson, R. (2003). Jurassic dipole low defined from land and sea  
704 data. *Eos Trans. AGU*, *84*, 362-366.
- 705 McFadden, P., & McElhinny, M. (1982). Variations in the geomagnetic dipole 2:  
706 statistical analysis of VDM's for the past 5 m.y. *Jour. Geomag. Geoelectr.*, *34*,  
707 163-189.
- 708 McFadden, P., & McElhinny, M. (1984). A physical model for paleosecular variation.  
709 *Earth Planet. Sci. Lett.*, *67*(19-33). doi: 10.1111/j.1365-246X.1984.tb05072.x
- 710 McFadden, P., & Merrill, R. (2000). Evolution of the geomagnetic reversal rate since  
711 160 Ma: Is the process continuous? *J Geophys Res-Solid Earth*, *105*, 28455-  
712 28460. doi: 10.1029/2000jb900258
- 713 Mercer, C. M., & Hodges, K. V. (2016). ArAr–A software tool to promote the ro-  
714 bust comparison of K–Ar and  $^{40}\text{Ar}/^{39}\text{Ar}$  dates published using different decay,  
715 isotopic, and monitor-age parameters. *Chemical Geology*, *440*, 148–163.
- 716 Moore, J. G., & Schilling, J.-G. (1973). Vesicles, water, and sulfur in Reykjanes  
717 Ridge basalts. *Contr. Mineral Petrol.*, *41*, 105-118. doi: 10.1007/bf00375036



- 718 Nagata, T., Arai, Y., & Momose, K. (1963). Secular variation of the geomagnetic to-  
719 tal force during the last 5000 years. *J. Geophys. Res.*, *68*, 5277-5282.
- 720 Olierook, H., Jourdan, F., Whittaker, J., Merle, R., Jiang, Q., Pourteau, A.,  
721 & Doucet, L. (2020). Timing and causes of the mid-Cretaceous global  
722 plate reorganization event. *Earth Planet. Sci. Lett.*, *534*, 1-13. doi:  
723 10.1016/j.epsl.2020.116071
- 724 Olson, P., Christensen, U., & Driscoll, P. (2012). From superchrons to secular vari-  
725 ation: A broadband dynamo frequency spectrum for the geomagnetic dipole.  
726 *Earth Planet. Sci. Lett.*, *319-320*, 75-82. doi: 10.1016/j.epsl.2011.12.008
- 727 Olson, P., & Hagay, A. (2015). Mantle superplumes induce geomagnetic superchrons.  
728 *Front. Earth Sci.*.
- 729 Paterson, G. (2011). A simple test for the presence of multidomain behavior dur-  
730 ing paleointensity experiments. *J. Geophys. Res.*, *116*(B10). doi: 10.1029/  
731 2011JB008369
- 732 Paterson, G., Tauxe, L., Biggin, A., Shaar, R., & Jonestrask, L. (2014). On im-  
733 proving the selection of Thellier-type paleointensity data. *Geochem. Geophys.*  
734 *Geosys.*, *15*(4). doi: 10.1002/2013GC005135
- 735 Pavón-Carrasco, F., & De Santis, A. (2016). The South Atlantic Anomaly: The Key  
736 for a Possible Geomagnetic Reversal. *Front. Earth Sci.*, *4*, 40. doi: 10.3389/  
737 feart.2016.00040
- 738 Perrin, M., & Schnepp, E. (2004). IAGA paleointensity database: distribution and  
739 quality of the data set. *Phys. Earth Planet. Int.*, *147*(2-3), 255-267.
- 740 Perrin, M., & Shcherbakov, V. (1997). Paleointensity of the Earth's magnetic field  
741 for the past 400 Ma: evidence for a dipole structure during the Mesozoic low.  
742 *J. Geomag. Geoelectr.*, *49*, 601-614. doi: 10.5636/jgg.49.601
- 743 Pick, T., & Tauxe, L. (1993a). Geomagnetic paleointensities during the Cretaceous  
744 normal superchron measured using submarine basaltic glass. *Nature*, *366*, 238-  
745 242.
- 746 Pick, T., & Tauxe, L. (1993b). Holocene paleointensities: Thellier experiments on  
747 submarine basaltic glass from the East Pacific Rise. *Jour. Geophys. Res.*, *98*,  
748 17949-17964.
- 749 Prévot, M., Derder, M. E. M., McWilliams, M., & Thompson, J. (1990). Intensity of  
750 the Earth's magnetic field: evidence for a Mesozoic dipole low. *Earth Planet.*  
751 *Sci. Lett.*, *97*, 129-139.
- 752 Riisager, P., Riisager, J., Zhao, X., & Coe, R. (2003). Cretaceous geomagnetic  
753 paleointensities: Thellier experiments on pillow lavas and submarine basaltic  
754 glass from the Ontong Java Plateau. *Geochem. Geophys. Geosyst.*, *4*(12), 8803,  
755 doi:10.1029/2003GC000611.
- 756 Santos, C., & Tauxe, L. (2019). Investigating the accuracy, precision, and cool-  
757 ing rate dependence of laboratory acquired thermal remanences during pa-  
758 leointensity experiments. *Geochem. Geophys. Geosys.*, *20*, 383-397. doi:  
759 10.1029/2018GC007946
- 760 Schmidt-Effing, R. (1975). El primer hallazgo de amonites en Améxicas en dicha  
761 reión. *Informe Semestral del Instituto Geográfico Nacional*, 53-61.
- 762 Schmidt-Effing, R. (1979). Alter und Genese des Nicoya Komplexes, einer ozeanis-  
763 schen Paläokruste (Oberjura bis Eozän) im südlichen Zentral Amerika. *Geol.*  
764 *Rundschau*, *68*, 457-494. doi: 10.1007/BF01820803
- 765 Selkin, P., & Tauxe, L. (2000). Long-term variations in paleointensity. *Phil. Trans.*  
766 *Roy. Soc. Lond.*, *358*, 1065-1088.
- 767 Sinton, C., Duncan, R. A., & Denyer, P. (1997). Nicoya Peninsula, Costa Rica:  
768 A single suite of Caribbean oceanic plateau magmas. *J. Geophys. Res.*, *102*,  
769 15,507-15,520.
- 770 Smirnov, A. V., & Tarduno, J. A. (2003). Magnetic hysteresis monitoring of Cre-  
771 taceous submarine basaltic glass during Thellier paleointensity experiments:  
772 evidence for alteration and attendant low field bias. *Earth Planet. Sci. Lett.*,

- 773 206(3-4), 571-585.
- 774 Steiger, R., & Jäger, E. (1977). Age and composition of the Rushan intrusive com-  
775 plex in the northern Sulu orogen, eastern China: petrogenesis and lithospheric  
776 mantle evolution. *Earth Planet. Sci. Lett.*, *36*, 359–62.
- 777 Tanaka, H., Kono, M., & Uchimura, H. (1995). Some global features of paleointen-  
778 sity in geological time. *Geophys. J. Int.*, *120*, 97–102.
- 779 Tarduno, J. A. (1990). Absolute inclination values from deep sea sediments: a reex-  
780 amination of the Cretaceous Pacific record. *Geophys. Res. Lett.*, *17*, 101–104.
- 781 Tarduno, J. A., Blackman, E., & Mamajek, E. (2014). Detecting the oldest geody-  
782 namo and attendant shielding from the solar wind: Implications for habitabil-  
783 ity. *Phys. Earth. Planet. Int.*, *233*, 68–87.
- 784 Tarduno, J. A., & Cottrell, R. D. (2005). Dipole strength and variation of the time-  
785 averaged reversing and nonreversing geodynamo based on Thellier analyses of  
786 single plagioclase crystals. *J. Geophys. Res.*, *110*, doi:10.1029JB003970.
- 787 Tarduno, J. A., Cottrell, R. D., & Smirnov, A. V. (2001). High geomagnetic in-  
788 tensity during the mid-Cretaceous from Thellier analyses of single plagioclase  
789 crystals. *Science*, *291*(5509), 1779–1783.
- 790 Tarduno, J. A., Cottrell, R. D., & Smirnov, A. V. (2002). The Cretaceous super-  
791 chron geodynamo: Observations near the tangent cylinder. *Proc. Natl. Acad.*  
792 *Sci. U. S. A.*, *99*(22), 14020–14025.
- 793 Tauxe, L. (2006). Long-term trends in paleointensity: The contribution of  
794 DSDP/ODP submarine basaltic glass collections. *Phys. Earth Planet. Int.*,  
795 *156*(3-4), 223–241.
- 796 Tauxe, L., Gee, J., Steiner, M., & Staudigel, H. (2013). Paleointensity results from  
797 the Jurassic: New constraints from submarine basaltic glasses of ODP Site  
798 801C. *Geochem. Geophys. Geosys.*, *14*(10). doi: 10.1002/ggge/20282
- 799 Tauxe, L., & Hartl, P. (1997). 11 million years of Oligocene geomagnetic field be-  
800 haviour. *Geophys. Jour. Int.*, *128*, 217–229.
- 801 Tauxe, L., & Kent, D. V. (2004). A simplified statistical model for the geomagnetic  
802 field and the detection of shallow bias in paleomagnetic inclinations: was the  
803 ancient magnetic field dipolar?
- 804 Tauxe, L., Shaar, R., Jonestrask, L., Swanson-Hysell, N., Minnett, R., Kop-  
805 pers, A. A. P., ... Fairchild, L. (2016). PmagPy: Software package for  
806 paleomagnetic data analysis and a bridge to the Magnetism Information  
807 Consortium (MagIC) database. *Geochem. Geophys. Geosys.*, *17*. doi:  
808 10.1002/2016GC006307
- 809 Tauxe, L., & Staudigel, H. (2004). Strength of the geomagnetic field in the  
810 Cretaceous Normal Superchron: New data from submarine basaltic glass  
811 of the Troodos Ophiolite. *Geochem. Geophys. Geosyst.*, *5*(2), Q02H06,  
812 doi:10.1029/2003GC000635.
- 813 Tauxe, L., & Yamazaki, T. (2015). Paleointensities. In M. Kono (Ed.), *Geomag-*  
814 *netism* (2nd Edition ed., Vol. 5, p. 461–509). Elsevier.
- 815 Thellier, E., & Thellier, O. (1959). Sur l'intensité du champ magnétique terrestre  
816 dans le passé historique et géologique. *Ann. Geophys.*, *15*, 285–378.
- 817 Thomas, D., Biggin, A., & Schmidt, P. (2000). A paleomagnetic study of Jurassic in-  
818 trusives from southern New South Wales: further evidence for a pre-Cenozoic  
819 dipole low. *Geophys. J. Int.*, *140*, 621–635.
- 820 Thomas, D., Rolph, T., Shaw, J., Gonzalez de Sherwood, S., & Zhuang, Z. (1998).  
821 Paleointensity studies of a late Permian lava succession from Guizhou  
822 Province, South China: implications for post-Kiaman dipole field behaviour.  
823 *Geophys. J. Int.*, *134*, 856–866.
- 824 Tournon, J., & Alvarado, G. (1997). *Mapa geológico de Costa Rica*. Ed. Tecnológica,  
825 Cartago.
- 826 Wang, H., Kent, D., & Rochette, P. (2015). Weaker axially dipolar time-  
827 averaged paleomagnetic field based on multidomain-corrected paleointensi-

- 828 ties from Galapagos lavas. *Proc. Nat. Acad. Sci.*, *112*, 15036-15041. doi:  
829 10.1073/pnas.1505450112
- 830 Whattam, S. A., & Stern, R. J. (2016). Arc magmatic evolution and the construction  
831 of continental crust at the Central American Volcanic Arc system. *Int.*  
832 *Geol. Rev.*, *58*(6), 653-686.
- 833 Wilkinson, M. D., Dumontier, M., Aalbersberg, I. J., Appleton, G., Axton, M.,  
834 Baak, A., . . . others (2016). The FAIR guiding principles for scientific data  
835 management and stewardship. *Scientific data*, *3*.
- 836 Yu, Y., Tauxe, L., & Genevey, A. (2004). Toward an optimal geomagnetic field in-  
837 tensity determination technique. *Geochem. Geophys. Geosyst.*, *5*(2), Q02H07,  
838 doi:10.1029/2003GC000630.
- 839 Zhu, R., Hoffman, K. A., Nomade, S., Renne, P. R., Shi, R., Pan, Y., & Shi, G. H.  
840 (2004). Geomagnetic paleointensity and direct age determination of the ISEA  
841 (M0r?) chron. *Earth Planet. Sci. Lett.*, *217*(3-4), 285-295.
- 842 Zhu, R., Hoffman, K. A., Pan, Y., Shi, R., & Li, D. (2003). Evidence for weak ge-  
843 omagnetic field intensity prior to the Cretaceous normal superchron. *Phys.*  
844 *Earth Planet. Int.*, *136*, 187-199.
- 845 Zhu, R., Lo, C., Shi, R. P., Pan, Y. X., Shi, G. H., & Shao, J. (2004). Is there  
846 a precursor to the Cretaceous normal superchron? New paleointensity and  
847 age determination from Liaoning province, northeastern China. *Phys. Earth*  
848 *Planet. Int.*, *147*(2-3), 117-126.
- 849 Zhu, R., Pan, Y., He, H., Qin, H., & Ren, S. (2008). Paleomagnetism and  $^{40}\text{Ar}/^{39}\text{Ar}$   
850 Ar age from a Cretaceous volcanic sequence, Inner Mongolia, China: Implica-  
851 tions for the field variation during the Cretaceous normal superchron. *Phys.*  
852 *Earth. Planet. Int.*, *169*, 59-75. doi: 10.1016/j.pepi.2008.07.025
- 853 Zhu, R., Pan, Y. X., Shaw, J., Li, D. M., & Li, Q. (2001). Geomagnetic palaeointen-  
854 sity just prior to the Cretaceous normal superchron. *Phys. Earth Planet. In-*  
855 *ter.*, *128*(1-4), 207-222.
- 856 Zijderveld, J. D. A. (1967). *A.C. demagnetization of rocks: Analysis of results.*  
857 Chapman and Hall.

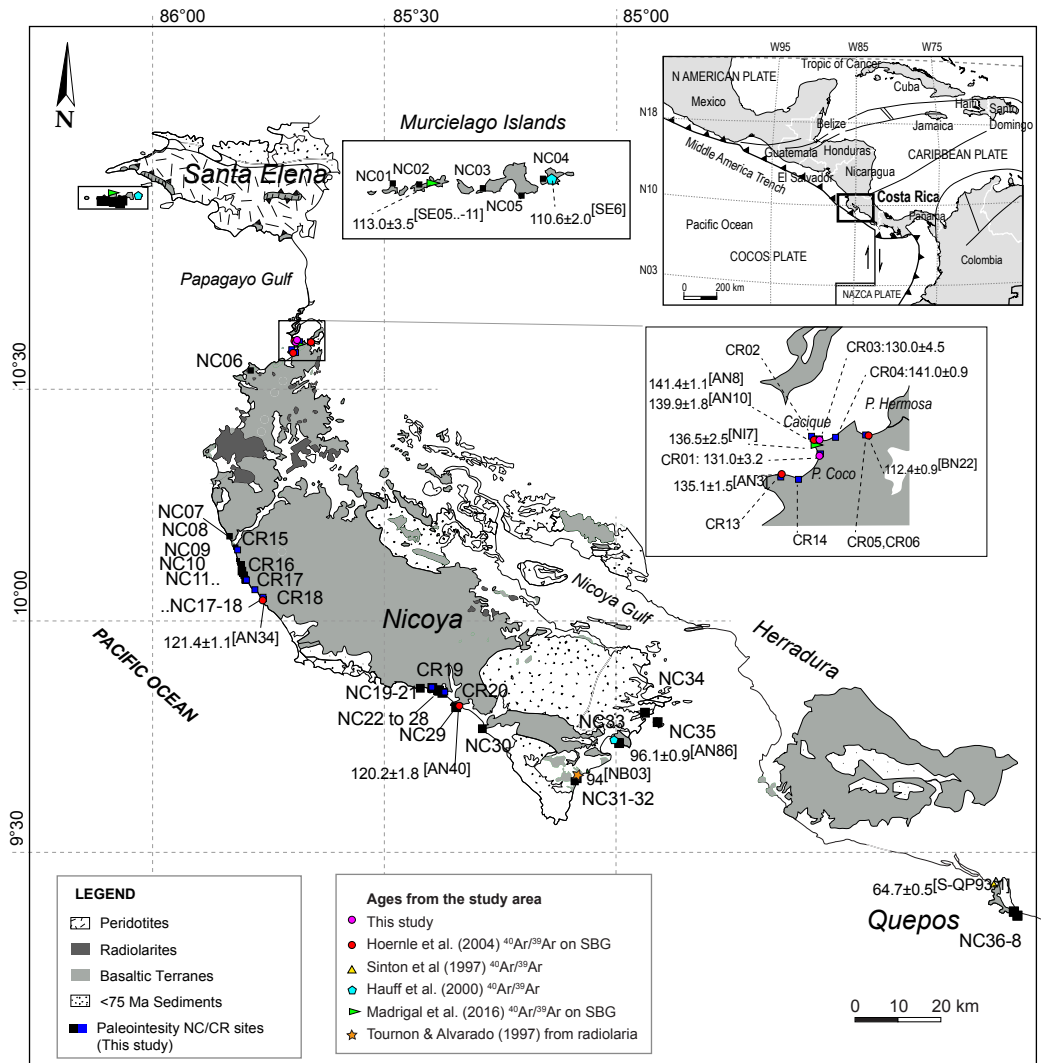


**Figure 1.** Geological map of the Nicoya Peninsula and surroundings, highlighting upper and lower crust terranes of the ophiolite, the sampling sites from previous studies and their age and the sites sampled for this study (black squares). Figure modified from Hauff et al. (2000). Sources of the  $^{40}\text{Ar}/^{39}\text{Ar}$  ages are Sinton et al. (1997) and Hoernle et al. (2004), compiled by Denyer and Baumgartner (2006) and Denyer and Gazel (2009). The CR-labelled paleointensity sites are from SBG samples provided by K. Hoernle, while the NC- sites are from SBG collected in 2017 for this study.



**Figure 2.** Sampling of the Basaltic Glass (SBG) in pillow lavas from the Nicoya Peninsula and Murciélago Islands (Costa Rica).

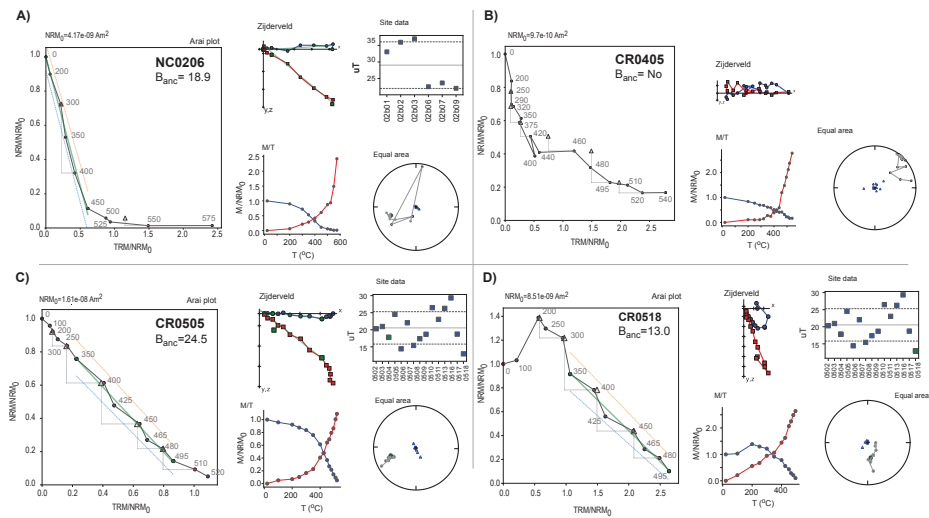


**Figure 3.** Examples of Arai plots (left hand plots in A-D) from four representative specimens, with relative Zijderveld (upper middle plots in A-D) magnetization vs. temperature (M/T; lower middle plots in A-D), equal area (lower right hand plots in A-D) and site-level plots (upper right hand plots in A-D). Numbers on the Arai plots are the Temperature steps (in °C), triangles show the directions of the pTRMs acquired in the laboratory field (along -z-axis of the specimens, i.e., the center of the diagram) and each blue and red circle a pair of ZI and IZ steps. Zijderveld diagrams are from un-oriented specimens and are plotted on the x-axis as the NRM direction with blue circles on the x,y plane and red squares in the x, z plane. The y-axis is with y,z as positive down. In the equal area plots, closed and open circles are the NRM directions in specimen coordinates with closed being the lower and upper hemisphere, respectively.

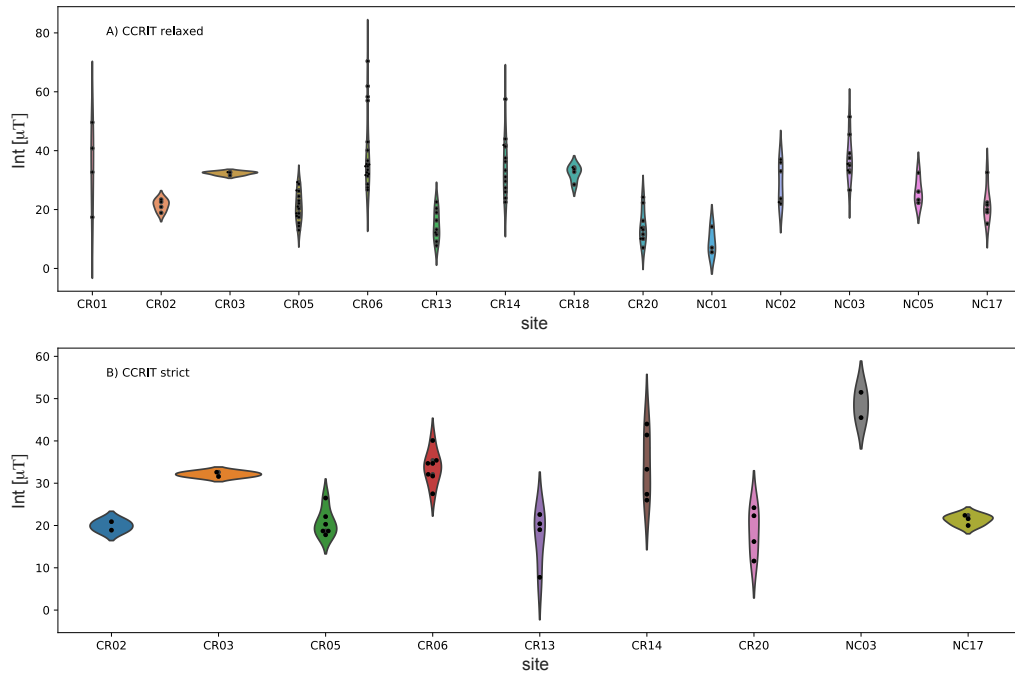


**Figure 4.** Violin plot showing intensity values for specimens (black dots) that passed the selection criteria along with kernel densities of their statistical distribution (colored areas), by using the A) CCRIT relaxed selection criteria, using a FRAC value greater than 0.3, and B) CCRIT strict criteria with a FRAC greater than 0.78.

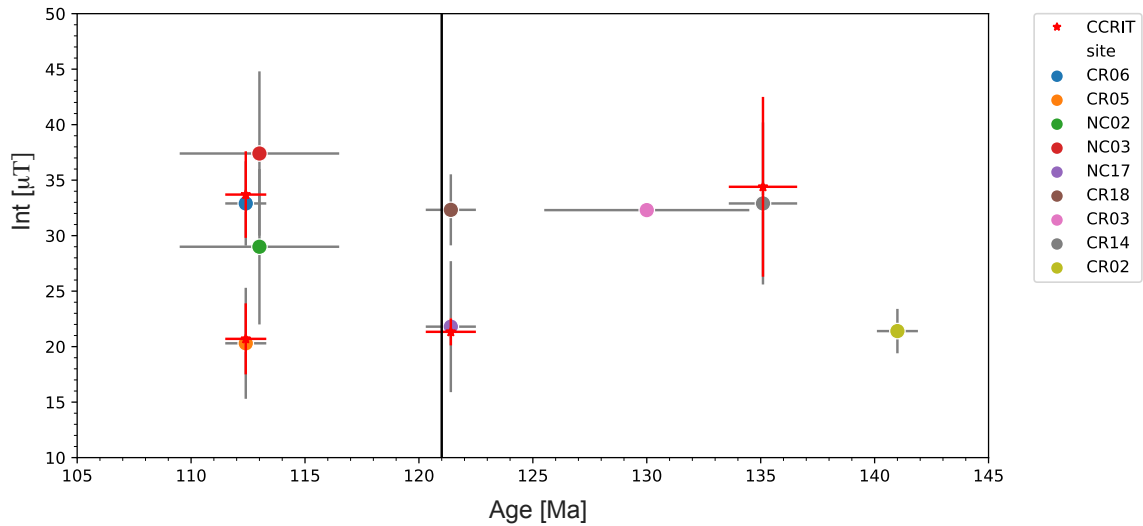


**Figure 5.** Paleointensity data (in  $\mu\text{T}$ ) and the error bars ( $1\sigma \mu\text{T}$ ) from Costa Rica sites vs Ages (Ma), obtained from  $^{40}\text{Ar}/^{39}\text{Ar}$  dating. Red stars are the sites for which the paleointensity values were obtained using the CCRIT strict set of criteria. The CNS onset interval is marked with vertical black line.

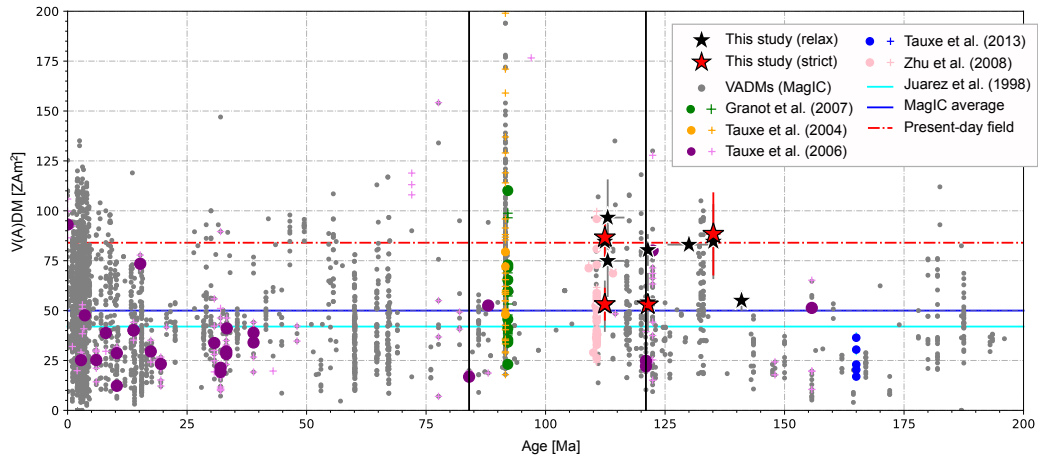


**Figure 6.** Black and red stars are the results of this study from Costa Rica (obtained with CCRIT relaxed and strict selection criteria, respectively). Grey dots represent the virtual (axial) dipole moments ( $V[A]DM$ ) available in the MagIC database spanning the last 200 Ma. The bounds of the Cretaceous Normal Superchron (CNS) are indicated with vertical black lines. The strength of the present dipole field is shown as a dashed red line, the solid blue line represents the average of all MagIC data, and the long-term average of Juarez and Tauxe (2000); Tauxe et al. (2013) is shown as a solid aquamarine line. Circles are the data from submarine basaltic glass (SBG) re-analysed using the same criteria as this study, while the data as presented by the authors are marked as crosses.